Characteristics of Structural Response to Ground Shocks

R P Dhakal and T-C Pan
Protective Technology Research Centre, School of Civil and Environmental Engineering, Nanyang Technological University, Singapore

ABSTRACT

This paper presents a conceptual discussion on structural response to ground shocks. Numerical parametric analyses are performed on a simplified linear structural model to investigate the special features of structural response brought by short duration, large amplitude and high frequency excitations, which are the basic characteristics of ground shocks induced by blasting. Nonlinear FEM analyses on a 2-storey RC frame subjected to ground shocks are carried out to qualitatively understand building response to blasting. This study shows that maximum structural response to blasting depends primarily on the amount of impulse, and it generally occurs after the major ground shock has ceased. To capture the maximum response, it is hence necessary to consider additional time duration beyond ground shock period in blasting analysis. It is found that the response in the forced-vibration phase includes high frequency vibration modes with small displacement but large acceleration, thus inducing high inertial shear force. However, the free-vibration response is dominated by lower frequency modes with larger displacement but smaller acceleration. Hence, buildings subjected to strong ground shocks might experience sudden shear failure of its components. Nevertheless, if a building strength is enough to avoid shear failure during the major shock, it may be damaged after the ground shock, and the extent of damage depends on the ground shock magnitude.

1. INTRODUCTION

Storing ordnances in the form of weapon, ammunition, and explosive is an integral part of the defence strategy of each country. Accidental blasting of such storages may cause significant damage to nearby structures. Hence, it is necessary to regulate the construction of residential structures in the vicinity of ammunition arsenals or underground explosive storage facilities. In other words, the closest permissible distance of residential buildings from such magazines, termed as the inhabited building distance (IBD), should be clearly manifested in the specifications.

In general, the current practice is based on NATO regulations [NATO 1999]. Equations proposed in these regulations to recommend IBD were based on analyses and tests conducted between the mid-1950s and the mid-1970s. Obviously, there are uncertainties in the present state-of-the-art, and further research in this field is necessary to identify the areas of technical uncertainties and to determine which of these could lead to significant economic paybacks when the degree of uncertainties is reduced. Due to space, costs and safety issues, extensive experimental investigation of structural response and damage due to blasting is usually not feasible. That is why only a few tests [Skjeltorp 1967, Murrell & Joachim

1996, Zhao et al. 1997] have been conducted, and experimental data in this field are scarce. This leaves numerical simulation as an alternative.

In order to estimate IBD reliably, the response of buildings to blasting-induced ground motion (BIGM) must be well understood. It is known that BIGM consists of short duration and large magnitude excitations of high frequency [Ma et al. 1998]. Due to these unique characteristics, building response to blasting is much different than that to earthquakes. In this pretext, one question remains unanswered: How should the conventional theories of structural dynamics be applied in blasting response prediction? In other words, researches addressing fundamental issues such as the qualitative influences of high frequency, short duration and large magnitude on the structural response to ground shocks are missing. The authors believe that conceptual guidelines based on the interaction between basic structural parameters and ground shock characteristics will be very much helpful in planning and implementing research strategies for further investigations. This paper tries to clarify these basic issues based on the response of a linear single degree of freedom (SDOF) system to BIGM, and also corroborates thus generated conceptual guidelines through nonlinear blasting analysis of a two-storey reinforced concrete (RC) frame.

2. TYPICAL GROUND SHOCK

The magnitude of a BIGM depends on many factors such as quality and quantity of explosives, depth of charge, surrounding soil properties, distance from the source, etc. As an extensive investigation with due consideration to all these parameters is out of scope, BIGM data simulated at different distances for one representative blasting condition [Ma et al. 1998] are used in this study. Altogether, six ground shocks corresponding to the horizontal and vertical motions simulated at 50, 100 and 150 m from a large-scale underground blasting source are considered. As a representative case, the acceleration time history of ground shock simulated in horizontal direction at 50 m surface distance and its Fourier transform are shown in Figure 1. Although the simulation is performed for 0.25 sec, the effective shock duration containing substantial acceleration amplitude is less than 0.05 sec. The peak ground acceleration (PGA) and the peak particle velocity (PPV) of this shock are 1220.19 m/s^2 and 0.978 m/s,

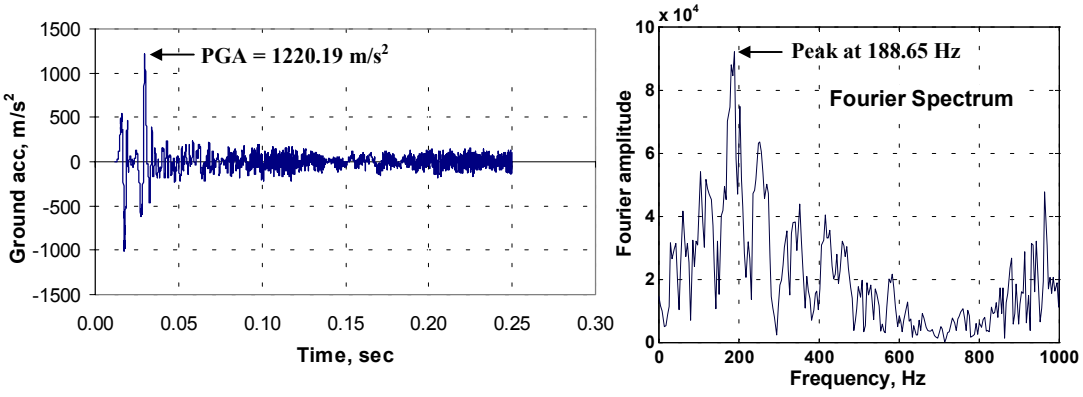

Figure 1. Typical BIGM simulated for horizontal direction at 50 m distance

Table 1. Characteristics of simulated BIGMs

Distance, m (Direction)	PPV, m/s	PGA, m/s^2	Frequency range, Hz	Dominant band and frequency at peak, Hz
50 (Horizontal)	0.978	1220.19	<1200	95-260 (188.65)
100 (Horizontal)	0.580	428.89	<800	50-225 (105.72)
150 (Horizontal)	0.426	343.16	<500	50-235 (103.65)
50 (Vertical)	0.874	1234.61	<700	120-285 (209.61)
100 (Vertical)	0.288	340.87	<600	30-400 (148.00)
150 (Vertical)	0.238	241.87	<500	40-320 (128.53)

respectively. Moreover, it includes significant higher frequency components, and the peak Fourier amplitude corresponds to 188.65 Hz.

Important parameters such as PPV, PGA, and frequency content of all six BIGM records are listed in Table 1. Interestingly, the vertical excitation is found to be significant and non-negligible in comparison with the horizontal one. From Table 1, it is evident that PPV and PGA of BIGMs decrease with the increase in distance but the rate of decrease becomes less prominent as the distance increases. It was also found that the very high frequency components gradually disappear as the distance increases, but the centre of dominant frequency band is only slightly affected within the simulated range. BIGMs have some unique features and hence are distinctly different from common seismic excitations. Firstly, the dominant frequency of a BIGM is significantly higher than that of a seismic excitation. Secondly, a BIGM lasts for a relatively short duration than a seismic excitation. Lastly, it has a much larger amplitude than that of a seismic excitation. These characteristics indicate that BIGMs are of impulsive nature, and a review of dynamic structural response to impulsive loads is helpful in understanding structural response to such ground shocks.

3. IMPULSE RESPONSE: REVIEW

Due to a very short loading duration, structural response to impulse can be divided into two phases: the forced-vibration phase (within the impulse duration), and the free-vibration phase (after the impulse has ceased). A structure subjected to impulse usually yields the maximum response in the free-vibration phase. Nevertheless, reliable response prediction in the forced-vibration phase is also important, as the displacement and velocity at the end of this phase will serve as the initial conditions for the free-vibration phase. Hereafter, responses of an SDOF system to impulsive ground shocks of four different shapes (sinusoidal, rectangular, symmetric and asymmetric triangular) are computed by solving the Duhamel integral [Clough and Penzien 1993]. In computations that follow, 5% damping ratio and PGA of 1000 m/s^2 are assumed for all ground shocks. Responses are computed for three shocks (with duration t_1 equal to 0.2, 0.1 and 0.04 sec), and six SDOF systems (with natural period T equal to 5.0, 2.0, 1.0, 0.5, 0.2 and 0.1 sec) are considered so that the ratio t_1/T ranges between 0.008 and 2.0.

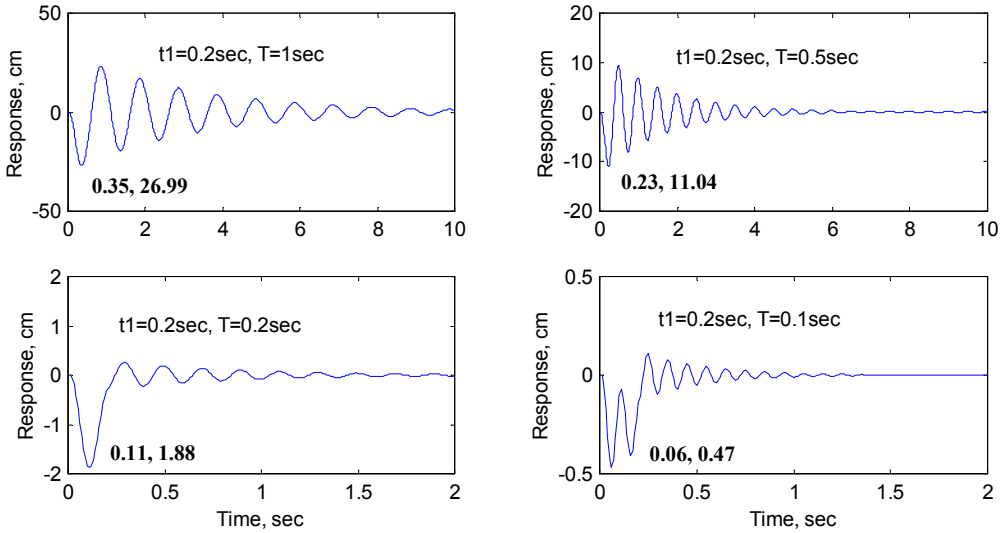

Figure 2. SDOF response to rectangular impulse (PGA = 1000 m/s^2)

The displacement response histories of SDOF systems with four different natural periods to a rectangular impulsive ground shock of 0.2 sec duration are shown in Figure 2. For the first two cases (T = 1.0, 0.5 sec), the maximum response occurs in the free-vibration phase, whereas for the third and the fourth cases (T = 0.2, 0.1 sec), response becomes maximum in the forced-vibration phase. Note that the maximum response is significantly smaller when it occurs in the forced-vibration phase. The results indicate that the maximum response does not depend separately on t_1 and T, rather it depends on the ratio t_1/T for all impulse shapes. For symmetrical impulses (sinusoidal, rectangular and triangular), the maximum response lies in the free-vibration phase if t_1/T is less than 0.5, and this critical ratio is 0.37 for asymmetric triangular impulsive load.

As different values of natural period T correspond to different mass and/or stiffness, the absolute displacement responses are not directly comparable. Hence, a generalized parameter called the maximum response factor R_{max}, which is defined as the ratio of the absolute maximum dynamic response to the static response, is used for comparison among different cases. For all impulse shapes, the relationships between R_{max} and t_1/T, also called the shock spectra, are drawn in Figure 3. As expected, the shock spectra corresponding to different impulse shapes are different from one another. Note that although R_{max} is unaffected when t_1/T is larger than 0.5, these two parameters are proportional for a lower t_1/T value. In other words, the response of a structure to a short-duration impulsive excitation depends primarily on the loading duration, which is directly proportional to the applied impulse. Hence for further clarification, R_{max} of the SDOF system with natural period of 1 sec is also plotted in Figure 3 against the total impulse; i.e. the area covered under the acceleration-time curve. Regardless of the impulse shape, the R_{max}-impulse relationship follows a common path for t_1/T smaller than the critical ratio. Nevertheless, this uniqueness no longer exists for larger values of t_1/T.

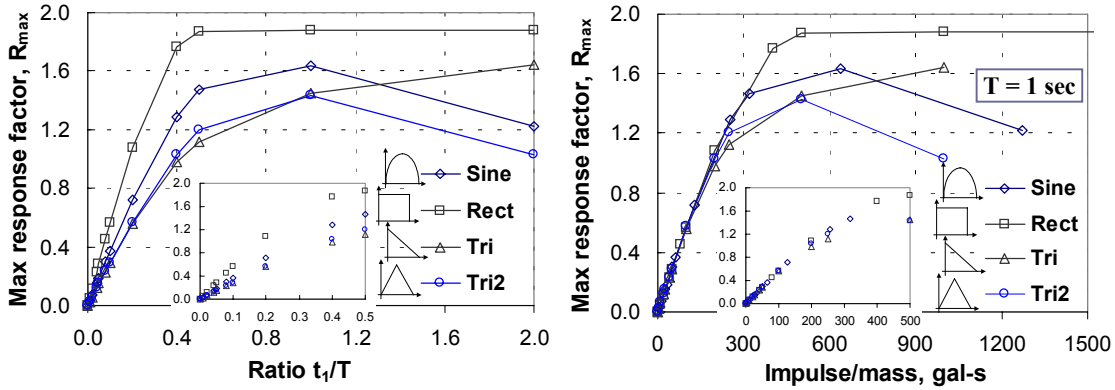

Figure 3. Maximum response of SDOF systems to impulse of different shapes

As the ratio of the effective duration of BIGM to the natural period of most civil engineering structures rarely exceeds the critical ratio, the maximum structural response to blasting usually occurs in the free-vibration phase. This fact advocates for the need to consider a longer duration than the actual ground excitation period in blasting analysis. Moreover, the maximum structural response to blasting depends mainly on the applied impulse.

4. EFFECT OF FREQUENCY

Next, special features brought by the dominant high frequency of BIGM in the structural response to blasting are explored. Basically, structural response is a combination of several modes, and each of these modes corresponds to a different frequency. Depending on structural properties and loading characteristics, different modes contribute differently to the overall response. Due to resonance, vibration modes of higher frequency dominate structural response to ground shocks. However, this is true only for the forced-vibration response within the loading duration, which is significantly short in the case of BIGM. The authors believe that in spite of higher frequency modes (closer to the dominant frequency of BIGM) dominating the structural response in the forced-vibration phase, vibration modes with a lower frequency (closer to the fundamental frequency of the structure) govern the response in the free-vibration phase. In other words, two important characteristics of structural response to BIGMs are: higher frequency modes dominating the forced-vibration response and lower frequency modes governing the free-vibration response. It is, therefore, necessary to understand qualitatively the relative contributions of vibration modes with different frequencies before drawing conclusions.

Hereafter, the response of a linear SDOF system with different natural periods to a typical simulated BIGM is computed to investigate the relative contribution of different modes. To cover all possible vibration modes, an SDOF system is assigned natural frequencies between 0.3 Hz and 300 Hz. To qualitatively represent resonance between the modal frequency and the loading frequency, natural frequency of 188.65 Hz, i.e. equal to the frequency corresponding to the peak of the Fourier spectrum of the applied BIGM, is assigned to one of the SDOF systems. For all computations that follow, damping

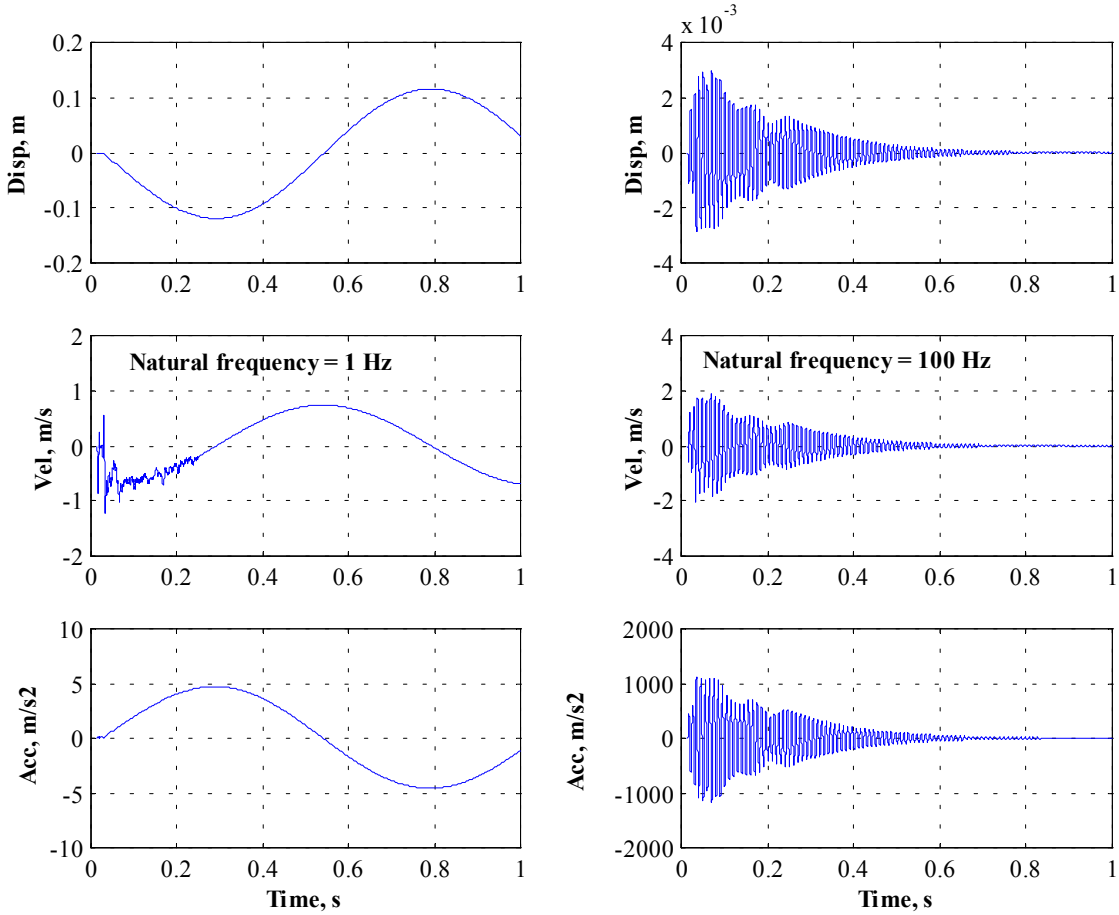

Figure 4. Response histories of SDOF system with different natural frequencies

Table 2. Effect of natural frequency on maximum response

Maximum Response	Natural frequency of SDOF system, Hz					
	0.3	1.0	10.0	100.0	188.65	300.0
Displacement, mm	414.2	119.4	9.2	3.0	3.1	0.65
Velocity, m/s	1.226	1.224	1.123	2.025	3.731	1.203
Acceleration, m/s^2	1.472	4.717	36.30	1176.4	4328.2	2331.0

ratio is assumed to be 1% of the critical. The displacement, velocity and acceleration responses of the SDOF systems with natural frequencies equal to 1 Hz and 100 Hz are shown in Figure 4.

As the effective loading duration is short (t_1 < 0.05 sec), the maximum response of the SDOF system with 1 Hz natural frequency (T = 1.0 sec) occurred in the free-vibration phase, and that with 100 Hz natural frequency (T = 0.01 sec) occurred in the forced-vibration phase. The maximum displacement of the SDOF system with 1 Hz natural frequency is significantly larger than that with 100 Hz. In contrast, the maximum acceleration of the SDOF system with 100 Hz natural frequency is much larger than that with 1 Hz. The maximum values of displacement, velocity and acceleration of the SDOF systems with different natural frequencies are listed in Table 2. As

the natural frequency of an SDOF system increases, the maximum displacement decreases. In spite of resonance with the dominant frequency of input BIGM, the maximum displacement of high frequency SDOF system is very small. However, the maximum acceleration increases with the increase in natural frequency.

Although real RC buildings are better represented by a multi degrees of freedom (MDOF) system with nonlinear properties, linear response of an SDOF system explains fairly the qualitative features brought by a vibration mode with frequency equal/close to the natural frequency of the SDOF system being considered. These results, therefore, indicate that the maximum acceleration is large and the maximum displacement is small if higher frequency modes are dominant, as in the forced-vibration response to BIGM. Similarly, the maximum acceleration becomes small, and the maximum displacement becomes large if the overall structural response is governed by lower frequency modes, as in the free-vibration response to BIGM. A large acceleration generates a significant inertia force, causing the shear force to increase considerably. On the other hand, a large displacement causes a larger strain that may damage the structure through cracking, yielding, etc. Hence, a structure subjected to blasting may be subjected to a significant shear force during the forced-vibration phase. If not, then it may undergo structural damage in the free-vibration phase.

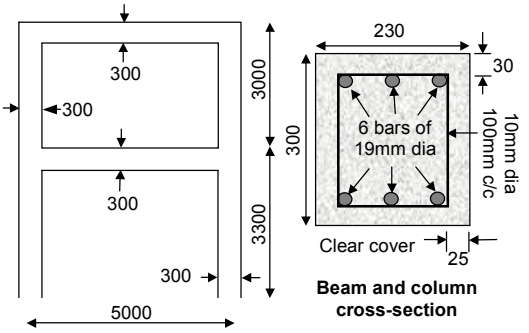

Figure 5. Target 2-storey RC frame

5. CASE STUDY: AN RC FRAME SUBJECTED TO BIGM

Earlier conclusions were drawn based on linear response of SDOF systems. In order to justify their validity in actual structures, nonlinear dynamic finite element analysis is conducted on a typical two-storey RC building frame subjected to the simulated BIGMs. This numerical investigation is meant to qualitatively investigate the influence of blasting on similar buildings. Though this study is not sufficient to explicitly formulate a general IBD recommendation, it certainly provides a fair idea regarding the response mechanisms and probable failure types of similar RC building frames when blasting occurs in the vicinity.

5.1 Target Structure

Layout of the representative two-storey RC building frame and its geometrical details are shown in Figure 5. This frame supports one side of a 5 m $\times$ 5 m $\times$ 150 mm slab resting on the beam in each floor. Density of 25 kN/m^3 is used to compute the self-weight of the RC frame and floor, and live load of 7.5 kN/m^2 is assumed to act on the floors. Following concrete properties are assumed: compressive strength = 30 MPa; tensile strength = 2 MPa; Poisson ratio = 0.2; compressive strain at peak strength = 0.24%; and

elastic modulus = 24.8 GPa. Similarly, the properties of steel reinforcement are adopted as follows: yield strength = 410 MPa; ultimate strength = 615 MPa; breaking strain = 5%; and Young modulus = 200 GPa. Shear capacity of the section taken as the sum of the shear contributions from concrete and web reinforcement turns out to be 171.9 kN. Similarly, moment capacity computed according to section analysis is equal to 107.75 kN-m. Assuming the beams to be rigid in axial direction and modelling the frame as a two-degrees of freedom system, frequencies for the first two global horizontal vibration modes are 1.8 Hz and 4.88 Hz, respectively. Similarly, global natural frequency in the vertical direction is approximately 27 Hz. According to preliminary computations based on a generalized SDOF system assuming both ends pinned, the local transverse vibrations of the beams and columns have fundamental frequencies around 4.3 Hz and 43.3 Hz, respectively.

5.2 Models Used in FEM Analysis

A three-dimensional nonlinear finite-element analysis program *Concrete Model in 3D* (COM3) [Maekawa et al. 1996] is used for numerical investigation. In COM3, nonlinear dynamic computation is based on the direct integration method. Columns and beams are discretized using frame elements, which are analysed by fibre technique. The two-storey RC frame is discretized into 60 elements (i.e. 10 elements for beams and columns in each storey) and each element consists of 220 parallel fibres. A fibre may contain either concrete only or both concrete and reinforcing bars depending on its position in the cross-section. Response of each fibre is computed using the averaged stress-strain relationships of concrete and reinforcing bars [Okamura and Maekawa 1991]. Note that these material models are nonlinear, cyclic and fully path-dependent. Moreover, issues such as concrete-rebar bond, cover concrete spalling and reinforcement buckling are given due consideration in formulating these models [Dhakal 2000]. These models have been experimentally verified at the material and structural levels with sufficient accuracy for static and dynamic analysis of reinforced concrete members [Okamura and Maekawa 1991].

In the analyses, the beam-column joint is modelled as part of a column member. An equivalent amount of mass is uniformly added throughout the length of the beams to account for the combined live and dead load coming from each floor. Total axial load on each column turns out to be 160 KN, which is around 7.7% of its axial capacity. Fixed supports are provided at the bases of both columns, and simulated BIGMs in the horizontal and vertical directions are applied simultaneously at these supports.

6. NUMERICAL RESULTS

6.1 BIGMs Simulated at 50 m

First, the RC frame is subjected to BIGMs simulated at 50 m from the blasting source. The displacement and acceleration response histories at different points in the frame are obtained from the output. Similarly, variation of the shear force induced at the base of the columns is also extracted. Lateral displacement

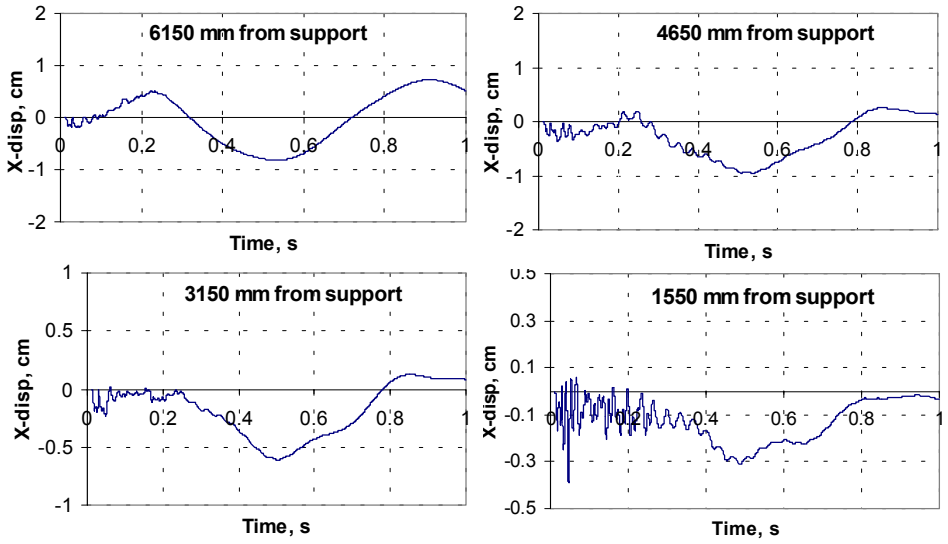

Figure 6. Lateral displacement histories of different points along the left column

response histories at different points in the left column are shown in Figure 6. As indicated earlier, the maximum response of lateral displacement occurs in the free-vibration phase due to the short BIGM duration. The maximum displacement at the top of the frame is around 9 mm, which corresponds to about 0.15% average storey-drift. As the displacement histories suggest, the roof vibrates in the fundamental global mode but oscillation of the second storey seems to include a higher order vibration mode, too. As expected, the displacement histories of column mid-heights in each storey indicate the presence of local vibration modes that have higher frequencies.

The existence of local vibration mode can also be illustrated from the absolute maximum lateral displacement profile of the two columns shown in Figure 7. The dashed straight line in Figure 7 represents the global mode, and column displacement from this line is the contribution of local modes, which is more prominent in the second storey. As the lateral displacements at different points in the column reach the maximum value almost simultaneously, the maximum displacement profiles also

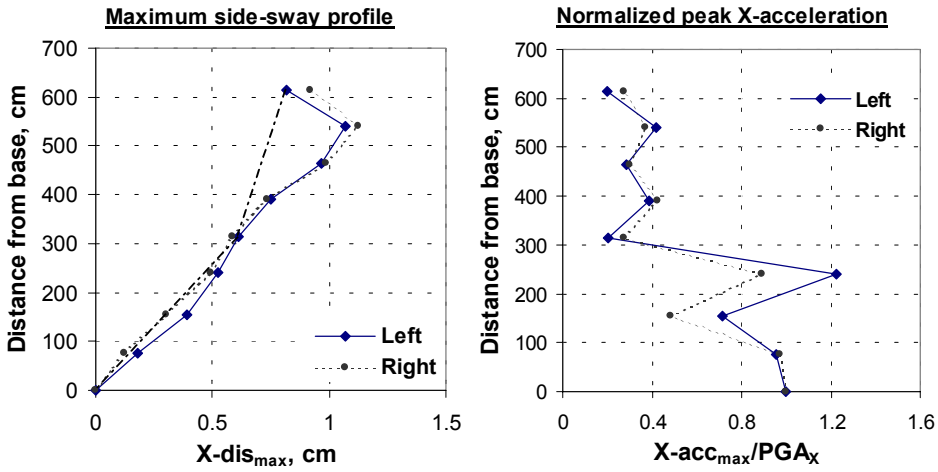

Figure 7. Normalized maximum lateral response profiles along the columns

represent the displaced shapes at the most critical condition. It can be observed that most of the global lateral displacement is concentrated in the first storey, and relative drift of the second storey is much smaller. Similarly, Figure 7 also shows the maximum lateral acceleration of different points in both columns normalized with respect to the horizontal PGA. It shows that the peak accelerations in the second storey and the roof are almost equal, and the peak accelerations at intermediate points in the columns are much larger than those at floor levels. This also corroborates that the columns respond with higher frequency modes than the floors.

Figure 8 illustrates the comparison of induced shear force at the base of both columns with the section shear capacity. In this analysis, shear force in the beam may be severer because of the larger inertia force owing primarily to the floor mass lumped in the beam. In actual response, the mass is distributed throughout the floor area, and the beam shear force would not be as detrimental. Nevertheless, shear force induced in the columns is not influenced by the distribution pattern of the dead and live loads. As is well known, column cross-sections at the base and near the joints are the most critical locations in terms of shear failure of such frames. The comparison in

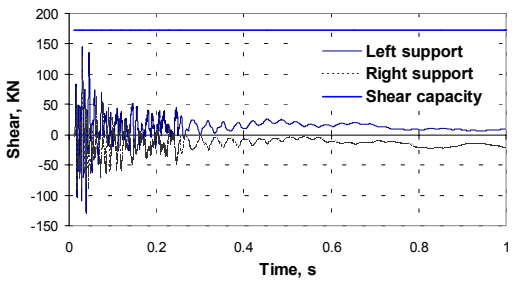

Figure 8. Shear force induced at the column bases (50 m BIGMs)

Figure 8 shows that the induced base shear is distinctly less than the shear capacity, i.e. 172 kN. Nevertheless, the maximum shear force, in this case, occurred in the left column just below the second storey. The maximum shear force induced at that location was equal to 165 kN, still slightly less than the predicted capacity. Note that the induced shear force becomes maximum during the forced-vibration phase, and the shear capacity corresponding to a higher loading rate is not necessarily equal to the one predicted earlier. During a high frequency excitation, the contribution of concrete may increase due to the increase in material strength, but the stirrups may not contribute as the shear cracks are expected to be perpendicular to the column axis rather than inclined at 45^{o}, as assumed in the truss analogy. Consequently, overall shear capacity may decrease slightly.

To qualitatively indicate the extent of damage, extreme strains of the outermost fibres in the beam and column cross-sections near the joints are shown in Figure 9. Stain histories of the extreme fibres at the most critical location along beam and column are also included in Figure 9. As can be seen, fibre strains at some locations are larger than yielding strain of the reinforcing bars ($\cong$2000 $\mu\varepsilon$), especially at the beam-ends and columns at the roof level. Hence, formation of plastic hinges at these locations cannot be ruled out. As strains in all locations exceed cracking strain of concrete ($\cong$150 $\mu\varepsilon$), cracks are expected to appear throughout the frame.

The response of the frame along vertical direction is not discussed in

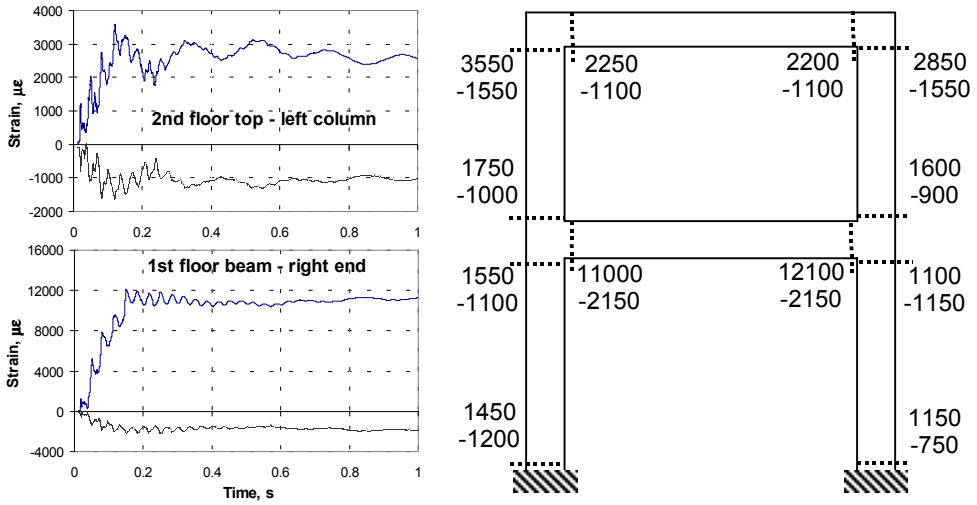

Figure 9. Extreme fibre strains induced in the frame due to 50 m BIGMs (in με)

detail because its magnitude is subjected to change depending on the distribution of floor loads. However, the qualitative nature of vertical response remains the same. Vertical displacement patterns of beams in the two floors are found to resemble with each other. Downward displacement is maximum at the centre of the beam but significantly smaller at the joints. Moreover, the peak vertical accelerations at the beam-ends are more than those at intermediate points along beam length. Both of these observations indicate that the joints follow the global vertical mode that has higher natural frequency due to the large axial stiffness of columns, but the beam vibrates in its local mode, which has a comparatively lower natural frequency.

6.2 BIGMs Simulated at 100 & 150 m

Next, the same RC frame is subjected to the BIGMs simulated at 100 m and 150 m, respectively. Though not shown in detail, responses in both cases are found to be qualitatively similar to those due to 50 m BIGMs. Needless to mention, the maximum shear force induced in the column is much less than the shear capacity, and the possibility of shear failure does not exist at all. Lateral displacements are smaller, e.g. average storey-drift due

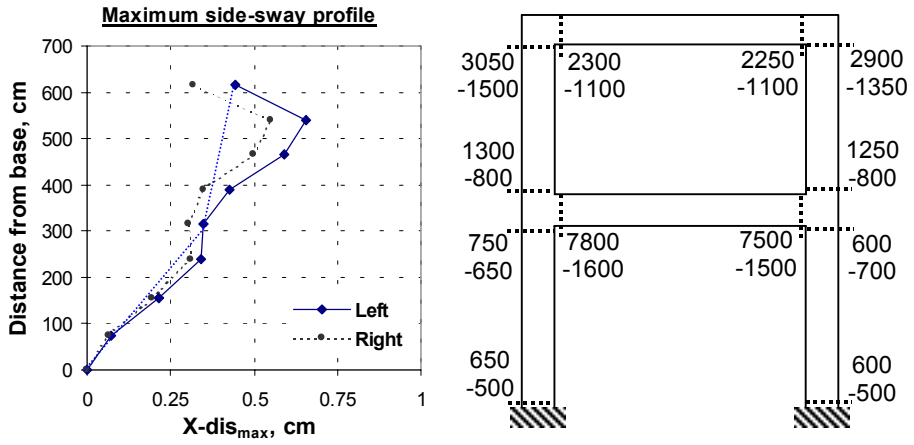

Figure 10. Maximum displacement and fibre strains in με due to 100 m BIGMs

to 100 m BIGMs is less than 0.1%. As in the previous case, high frequency vibration modes could be noticed in the response histories. Figure 10 shows the maximum displacement profiles of the columns and the extreme strains in the outermost fibres at some critical locations for 100 m BIGMs. In spite of the small storey-drift, strains are found to be non-negligible, especially at the beam-ends and columns at the roof level. Localized damages are expected at the beam-ends in the first storey and some sporadic cracks are expected in other parts as well. For 150 m BIGMs, numerical results show that strains at almost all locations are less than yielding strain. Hence, the frame does not experience much damage although a few fine cracks may appear at some locations. These numerical results indicate that the typical two-storey RC building frame is moderately damaged when subjected to the simulated BIGMs at a distance of 50 m, but it can bear without much damage the simulated BIGMs at 100 m or more.

6.3 Extrapolated Severer BIGMs

Next, the same RC frame is subjected to two times the ground shock data simulated for 50 m distance from the blasting source. These extrapolated data may represent either one or both of the following conditions: (i) ground shock at a closer distance from the blasting source, and (ii) ground shock induced by a larger amount of explosive.

As shown in Figure 11, the maximum lateral displacement at the roof level is around 2.0 cm (i.e. 0.33% average storey-drift). The maximum tensile and compressive fibre strains in some locations of the frame are also illustrated in Figure 11. As expected, it can be noticed that strains are much larger than in the previous cases, and the frame might experience severe damage. It is to be reminded that the strains become maximum in the free-vibration phase whereas the induced shear force becomes maximum during the forced-vibration phase. The shear force induced at the base of the columns is compared with the shear capacity in Figure 12. It can be observed that base shear is higher than the capacity. Considering that the maximum shear force in the column just below the second storey is even higher, it can be said that shear failure is highly likely to take

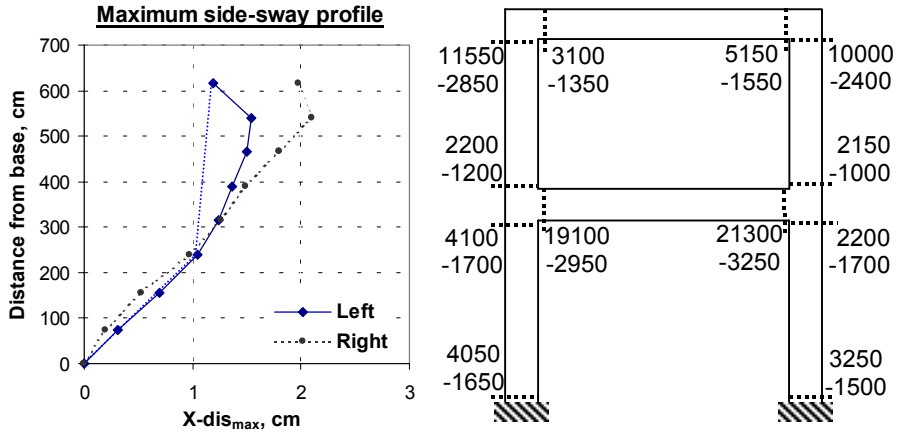

Figure 11. Maximum displacement and fibre strains in με (50 m BIGM×2)

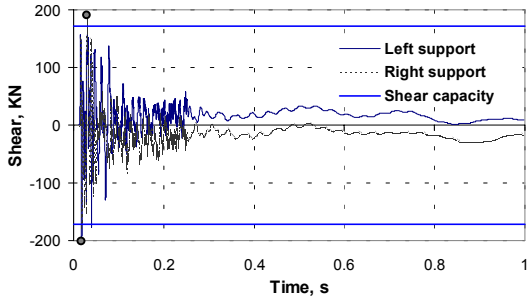

Figure 12. Shear force induced at the column bases (50 m BIGMs×2)

place in the forced-vibration phase. The frame may collapse due to sudden shear failure before being damaged due to larger strains in the free-vibration phase. Note that the frame did not show signs of shear failure due to 50 m BIGMs although sub-critical structural damage could be observed in the free-vibration phase.

6.4 Qualitative Damage Attenuation

Based on these numerical results, overall safety of the RC building frame located at various distances from a blasting source of different magnitude can be qualitatively assessed. Figure 13 illustrates schematically the qualitative relationship between the extent of damage of the frame and the distance between the frame and the blasting source. The solid line (curve 1) in Figure 13 corresponds to the damage corresponding to a simulated explosive quantity, say Q_s. The other three dashed lines in the figure represent cases with more (curve 2) and less (curves 3 and 4) amount of explosives. Safety of the frame far from the blasting source is always guaranteed regardless of the amount of explosive. For closer distances, two damage mechanisms are identified. At a very close distance from the blasting source, the frame may undergo a sudden shear failure of some of its components during the forced-vibration phase, as described by curves 1 and 2. As this type of failure is governed by induced shear force that in turn depends on input energy or impulse, the frontier of shear failure zone D_{sh} depends primarily on the amount of explosive and the shear capacity of its components. For considerably small quantity of explosive as described by curves 3 and 4, the shear failure zone may not exist at all. The frame located outside the shear failure zone D_{sh} can safely overcome the forced-vibration phase, but may still

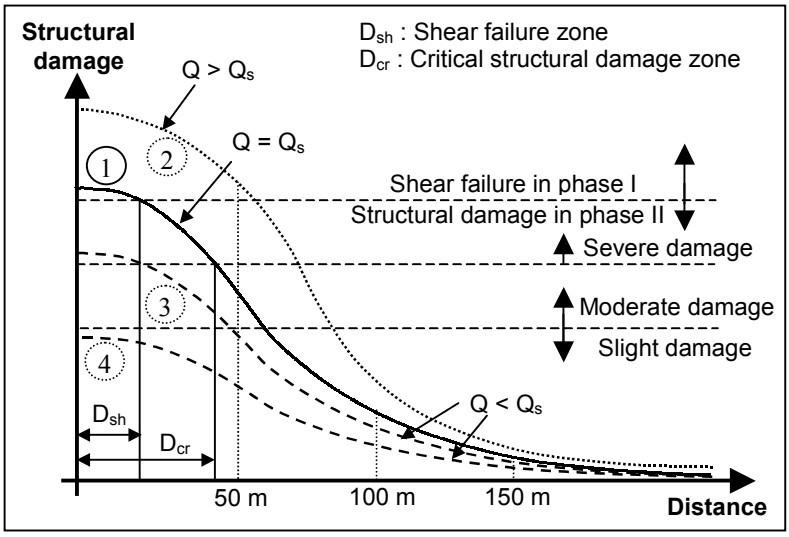

Figure 13. Schematic damage attenuation curve for the 2-storey RC frame

experience severe damage in the free-vibration phase if it is inside the critical structural damage zone D_{cr}.

7. CONCLUSIONS

Fundamental concepts of structural dynamics are employed to explain the characteristics of structural response to underground blasting. BIGM has some special characteristics such as high frequency, large amplitude and short duration. Parametric studies based on the response of an SDOF system to BIGM were carried out to highlight the influence of these special features in various structural response parameters. Due to the impulsive nature of BIGMs, the maximum structural response usually occurs after the major ground shock; i.e. in the free-vibration phase and is proportional to the total impulse applied. Hence, analyses aimed to predict structural response to blasting are recommended to cover a time domain much longer than the ground shock duration, and computations only within the BIGM duration will underestimate the maximum structural response.

The forced-vibration response to a BIGM is dominated by higher frequency vibration modes, whereas the free-vibration response in mainly governed by the lower frequency vibration modes. Higher frequency modes cause a smaller displacement but a larger acceleration, thus causing a high shear force in the forced-vibration phase. On the other hand, lower frequency modes cause a larger displacement and a smaller acceleration, thus increasing the possibility of structural damage in the free-vibration phase. Hence it can be concluded that for structures closer to a larger-scale blasting source, sudden shear failure may take place during the forced-vibration phase due to the excessive input energy or impulse. Note that the range of shear failure zone D_{sh} and the critical structural damage zone D_{cr} depend on the scale of blasting and the structural toughness. For example, an explosion may be hazardous for a weak building and, at the same time, harmless for a stronger building.

8. REFERENCES

- Clough, R.W. and Penzien, J., *Dynamics of Structures*, McGraw-Hill, Second Edition, 1993.
- Dhakal, R.P., *Enhanced Fiber Model in Highly Inelastic Range and Seismic Performance Assessment of Reinforced Concrete*, Doctoral Dissertation, Department of Civil Engineering, The University of Tokyo, 2000.
- Maekawa, K., Irawan, P. and Okamura, K., “Three-Dimensional Constitutive Laws of Reinforced Concrete”, *Proceedings of the International Conference on Applied Concrete Mechanics APCOM*, Seoul, 1996.
- Ma, G., Hao, H. and Zhou, Y.X., “Modelling of Wave Propagation Induced by Underground Explosion”, *Computers and Structures*, 1998 (3-4), Vol. 22, pp. 283-303.
- Murrell, D.W. and Joachim, C.E., *The 1996 Singapore Ground Shock Test*, Waterways Experiment Station, Department of Army, Vicksburg, 1996.
- North Atlantic Treaty Organization, *Manual on NATO Safety Principles for the Storage of Ammunition and Explosives*, Document AC/258-D/258, Brussels, 1999.

- Okamura, H. and Maekawa, K., *Nonlinear Analysis and Constitutive Models of Reinforced Concrete*, Gihodo, Tokyo, 1991.
- Skjeltorp, A., *Underground Ammunition Storages: Model Tests to Investigate External Safety Distances*, Fortifikatorisk Notat 36/67, Norwegian Defence Construction Service, Oslo, 1967.
- Zhao, J., Wu, Y.K., Cai, J.G., Chen, S.G. and Zhao, Y.H., *Small–scale Ground Shock Tests at the Mandai Quarry*, Technical Report to the Lands and Estates Organization, Ministry of Defence, Singapore, 1997.